Time evolution of thermal conductivity and intrinsic permeability of a snow cover

GEOQuébec 2015
Challenges from North to South
Des défis du Nord au Sud

Olivier Lachance, Jean Côté
Département de génie civil et de génie des eaux – Université Laval, Québec, QC, Canada

ABSTRACT
This paper presents the experimental results of a study on the time-evolution of the intrinsic permeability, thermal conductivity and porosity of a single snow layer. Undisturbed snow batches were collected at Laval University in the winter of 2014 at weekly intervals. They were later reworked to produce samples of different porosities. The experimental results obtained for the different samples ranged from 3.59 x 10^{-9} to 8.71 x 10^{-11} m^2 for the permeability and from 0.089 to 0.372 W/mK for conductivity with porosity varying from 0.46 up to 0.80. A temporal evolution of the relation permeability-porosity has been observed and an effective radius corresponding to each snow batch and sample was obtained using an existing permeability model (Calonne et al. (2012)). That radius has allowed the quantification of the temporal evolution process. A structure effect resulting from compaction has also been noticed on the thermal conductivity measurements of fresh snow samples.

RÉSUMÉ
Cet article présente les résultats expérimentaux de l’évolution temporelle des relations entre la perméabilité intrinsèque, la conductivité thermique et la porosité d’une couche de neige. Des lots de neige ont été recueillis à l’Université Laval à l’hiver 2014 à intervalles hebdomadaires et des échantillons remaniés de différentes porosités y ont été extraits. Les plages de valeurs des résultats expérimentaux obtenus sont de 3.59 x 10^{-9} à 8.71 x 10^{-11} m^2 pour la perméabilité intrinsèque et de 0.089 à 0.372 W/mK pour la conductivité thermique pour des porosités de 0.46 à 0.80. Une évolution temporelle de la relation perméabilité-porosité a été observée et quantifiée grâce au calcul d’un rayon effectif pour chaque échantillon effectué à l’aide d’un modèle existant (Calonne et al. (2012)). Un effet de structure résultant de la compaction a également été remarqué sur la mesure de la conductivité thermique d'échantillons de neige fraiche.

1 INTRODUCTION

In cold region environments with snow precipitations, ice crystals within the snow cover are exposed to temperature gradient which produces water vapor displacement from sublimation and condensation. These processes result in alteration of the structure and size of the snow grains and are the cause of snow metamorphism. The physical properties are thus greatly affected by metamorphism (Colbeck et al. 1990, Domine et al. 2003, Legagneux et al. 2003, Taillandier 2006, Morin et al. 2013). Although many studies investigate the evolution of the snow grain size and specific surface area (SSA) over time (Sturm and Benson 1997, Legagneux et al. 2003, Taillandier 2006), only a few have reviewed the impact of aging on heat and mass transfer properties (Morin et al 2010, Domine et al 2013).

The objectives of this study are to characterize the evolution of snow properties used in heat and mass transfer, the intrinsic permeability and thermal conductivity, and to suggest a relationship to quantify that maturation for the conditions encountered in the province of Quebec. The paper presents the experimental setups for the measurement of intrinsic permeability using a double-chamber air permeameter and for the thermal conductivity using a needle probe. The experimental results for compacted snow specimen sampled at different times are also shown and compared with previous experimental values and models. The results are discussed in terms of the equivalent sphere radius using a model proposed by Calonne (2012) to fit the experimental data sets. It was then possible to link the equivalent snow grain size and specific surface area to the age of the snow and to compare with available data from the literature. Finally, an observable compaction effect on thermal conductivity over time is discussed.

2 EXPERIMENTAL PROGRAM

2.1 Experimental setup

Figure 1 shows the apparatuses used in this study for both measurements on snow samples. The double-chamber air permeameter (Shimizu 1970, Hardy and Albert 1993, Arakawa et al. 2009) that was designed for the laboratory testing of snow samples is presented in Figure 1A. Compressed air is supplied at about 20 °C then cooled through a copper coil and fed to a 23 liters tank kept at testing temperature (-10 °C). It is then routed to a control and measurement panel at the same temperature condition. Differential pressure is measured using a PX654-0.5D5V, a 0 to 124.5 Pa differential pressure sensor from Omega. The mass flow meter used in this study is an AWM5104VN from Honeywell. It has a range of 0 to 20 SLPM (Standard Liter per Minute). Temperature in the insulated box is monitored with a ntc thermistor and controlled throughout the tests to maintain the ambient temperature at -10 °C.

The sample holder consists of three cylindrical pieces of 95 mm diameter, the head, the core and the base, which assemble together sealed by two O-rings. The head cylinder is equipped with an inner cylinder of a diameter of 45 mm and a total length of 5 mm longer than the outer cylinder. This allows insertion in the sample forming a relative separation between inner and outer sections at the top of the sample. This feature tends to minimise the impact of a bad contact between the sample and the holder as well as to reduce sample alteration at the cylindrical surface. The area of flow measurement is then defined by the inner wall. A layer of fiberfill has been added in both sections of the head cylinder acting as a diffusion filter to homogenize the velocity profile and reduce the risk of sample damaging from a narrow air jet supply. The sample lies on a fine rigid wire mesh set on the base of the sample holder. The measurement process starts with the adjustment of the flow rate in the inner cylinder to the desired value. Then the pressure differential is set to zero between the inner and outer cylinder. Subsequently, a three-way valve is positioned to measure differential pressure between the inner cylinder at the top and the bottom of the sample to obtain the pressure gradient, knowing the sample height. The procedure is repeated about ten times for various flow rates. The intrinsic permeability can be calculated using Darcy's law applied to this situation:

$$u = \frac{k}{\mu} \nabla P \qquad [1]$$

where u is the Darcy's velocity (m/s) calculated by dividing the mass flow rate by the air density and by the area of the inner section, k is the intrinsic permeability (m^2), μ is the dynamic viscosity of air (Pa·s) and ∇P is the pressure gradient in (Pa/m).

The double chamber air permeameter and procedure have been successfully validated by the measurement of 1 mm and 4 mm diameter glass beads and 2 mm diameter lead beads at -10 °C. The results were consistent with theoretical values obtained using the Kozeny-Carman equation (Carman 1956).

The measurement of thermal conductivity is performed using the transient line source method with the needle probe shown in Figure 1B, withdrawn from the sample for the needs of the picture. The main sensor of the probe consists of a type K thermocouple, the hot joint being situated at the middle of the needle and the cold joint in the handle. A PT1000 RTD temperature sensor positioned near the cold joint allows copper wiring from the handle to the acquisition. A 83.94 Ω/m heating wire running through the entire needle length emulates a perfect line source. This measurement method has been used in many previous studies (Jaafar and Picot 1970, Sturm and Johnson 1992, Côté et al. 2012, Lachance et al 2013 and Lachance 2014). The thermal conductivity measurement procedure used in this study consists in the application of a linear heat pulse of approximately 0.85 W/m for 110 seconds while monitoring the needle temperature rise with the thermocouple hot joint. The following simplified equation is used to compute the conductivity:

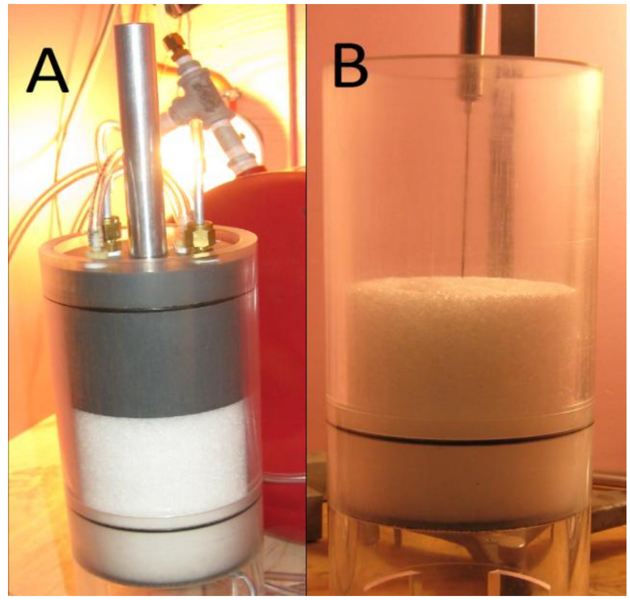

Figure 1. Photo of the actual experimental setups. A: Air permeameter for intrinsic permeability, B: needle probe for thermal conductivity measurement.

$$\lambda = \frac{Q}{4 \cdot \pi \cdot m} \qquad [2]$$

where Q is the linear heat flux (W/m) applied by the heating wire to the sample and m is the semi-logarithmic slope of the temperature rise (K).

The measurement procedure has been successfully validated by the measurement of the thermal conductivity of glycerol, which has a known value of 0.29 W/mK at 20 °C.

2.2 Sampling and samples preparation

A total of 6 sampling were made at Laval University at different time during the winter of 2014 from snow resulting from a single snowfall (January 26th). Figure 2 shows meteorological information near the sampling site. The sampling dates are represented with coarse dashed line, the daily average temperature and height of snow on the ground with a solid line and the amount of rain with a finely dotted line (bottom right vertical scale). The winter of 2014 in Québec city was very special since the temperature constantly remained below 0°C from mid-January to early April with an average temperature of -10°C. Moreover, there was higher temperatures and rain precipitation early January which resulted in a hard and thick ice crust. This ice layer was used as point of reference of height for snow sampling. In fact, for each sampling, snow was collected at a height of 0 cm to about 10 cm above the ice, which made possible to study the in situ development of the snow layer. Specimens were also gathered within an area of about 100 m^2 to assure uniformity. The average total snow height was 0.86 m with an average thermal gradient of -11.7 °C/m.

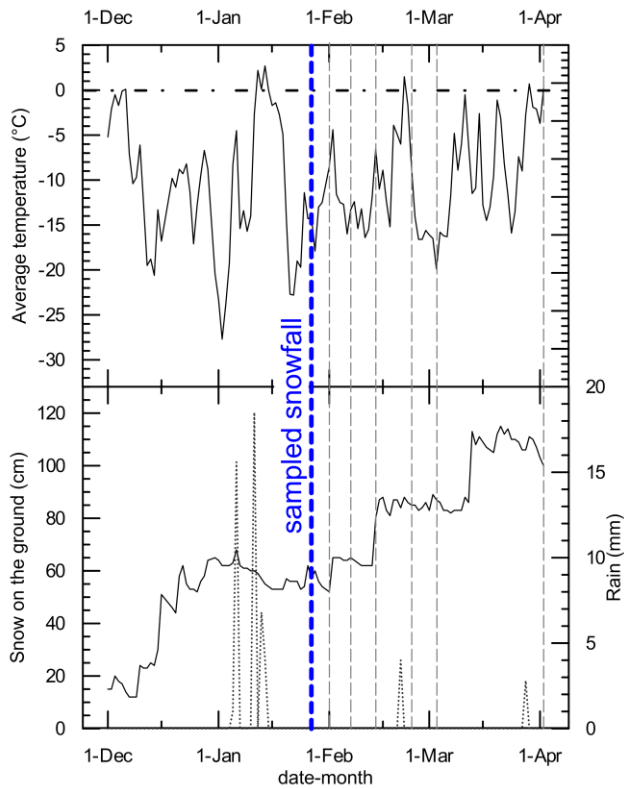

Figure 2. Meteorological data for the winter of 2013-2014.

Collected snow batches were gently poured in temperature conditioned bags and then placed within thermally insulated boxes in a cold room at a temperature of about -18°C. As noted in Table 1, 41 samples were made out of 7 batches at different sampling dates. Various sample densities were obtained by static consolidation under uniform loading in the cell of the permeameter.

3 EXPERIMENTAL RESULTS

3.1 Typical measurements

Typical experimental data for an intrinsic permeability measurement are shown in Figure 3 for a sample from January 27th batch tested January 30th at -10°C with a porosity of 0.75. The Darcy velocity (vertical axis) was set to successive steps while the resulting pressure gradient (horizontal axis) was recorded. The intrinsic permeability can be obtained with Darcy's law (Equation 1) knowing the slope of the curve in Figure 3 and the dynamic viscosity at test temperature. In that case, the slope is 2.65 x 10^{-5} m^2/(Pa·s) with a viscosity of 1.66 x 10^{-5} Pa·s, therefore the intrinsic permeability is 4.40 m^2. The Darcy velocity was maintained below 0.055 m/s as nonlinear phenomenon occurs at higher velocities. That is the limit of application of Darcy's law for the apparatus where it shifts to a Darcy-Forchheimer flow. These results are in agreement with Bader et al. (1939), Shimizu (1970), Hardy and Albert (1993), who had experienced these effects at 0.06 m/s, 0.047 m/s and 0.056 m/s respectively.

A typical thermal conductivity measurement is presented in Figure 4 and 5 for the exact same sample as it was performed in the same cell immediately after the permeability measurement. Figure 4 shows the total temperature rise in the sample versus time in a logarithmic scale. A typical total temperature rise of about 2.5°C is generally reached after testing, depending on the thermal conductivity of the sample. The 30 first seconds are discarded since this period corresponds to the warming phase of the needle as well as time over 80 seconds as it is more likely to experience unwanted effect such as heat wave reflection from the cell wall. Given the data from Figure 4, equation 2 is used to compute the conductivity. The conductivity obtained in this manner is 0.132 W/m·K for a heat input of 0.835 W/m and a slope of 0.5031.

For each sample, several measurements were made at intervals of an hour to get an average value and reduce the effect of data scattering (Côté et al. 2012). The ambient temperature is maintained at -10 °C during the whole process. An example of successive measurements for the same sample is shown in Figure 5 with the resulting average of 0.13 W/mK with a standard deviation of 4.6 %.

The intrinsic permeability and thermal conductivity measurement results are summarized in Table 1 and further presented in sections 3.2 and 3.3.

Table 1. Summary of experimental results sorted by sampling date.

Sampling date	Number of samples	Porosity range	λ range (W/m·K)	k range x10^{-10} (m^2)
27 Jan	6	0.65–0.80	0.09-0.22	0.9-7.5
31 Jan	7	0.58-0.75	0.10-0.26	1.8-14.2
07 Feb	6	0.49-0.65	0.14-0.33	2.4-16.8
14 Feb	6	0.45-0.63	0.14-0.36	1.9-16.8
24 Feb	6	0.42-0.58	0.24-0.48	1.8-13.2
03 Mar	5	0.46-0.60	0.13-0.44	3.0-15.6
02 Apr	5	0.46-0.60	0.19-0.37	6.0-35.9

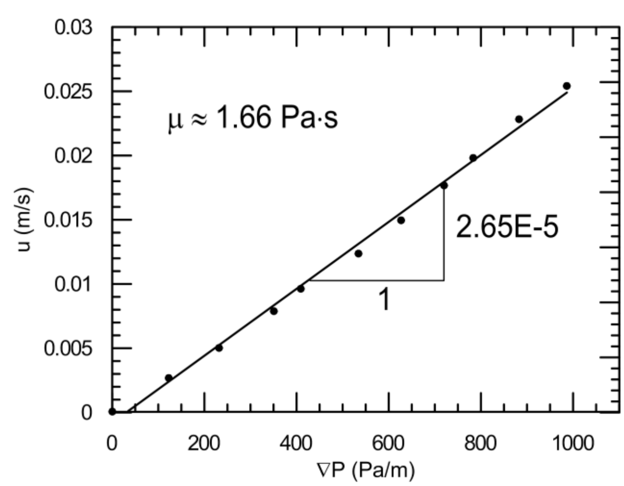

Figure 3. Typical permeability measurement. Pressure gradient across the sample versus the Darcy velocity.

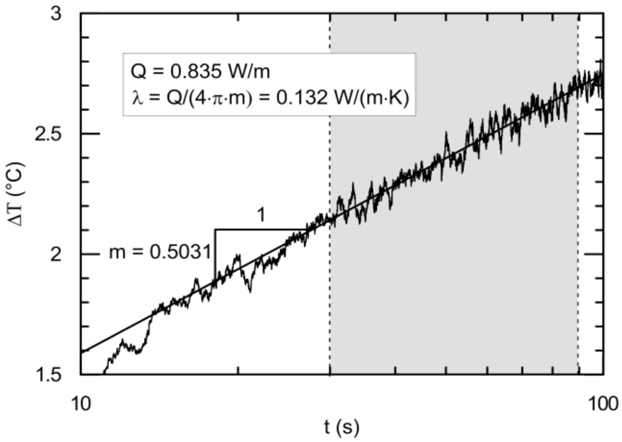

Figure 4. Typical thermal conductivity measurement. Temperature rise in the needle versus time (logarithmic scale).

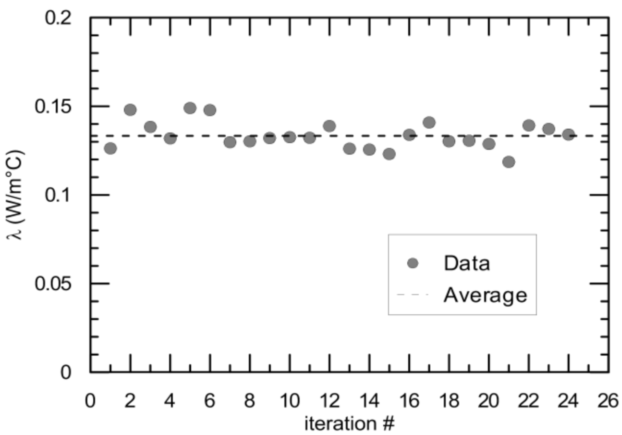

Figure 5. Consecutive thermal conductivity measurement for a single sample.

3.2 Intrinsic permeability measurements

Intrinsic permeability measurements are shown in Figure 6 for each sampling date as a function of porosity. Permeability values between 0.9 x10^{-10} m^2 and 35.9 x10^{-10} m^2 were obtained for porosity varying from 0.42 to 0.80. These results agree well with data sets from previous studies (Shimizu 1970, Hardy and Albert 1993, Sommerfeld and Rocchio 1993, Arakawa et al. 2009) shown by the pale gray dots in Figure 6.

As anticipated, the intrinsic permeability for each sampling date has a clear tendency to increase with porosity, as the air flow is less restricted in a looser material. For example, the results obtained for the batch of January 27th (next day of snow fall) shown in red clearly illustrates this trend where permeability is equal to 7.7 × 10^{-10} m² at a porosity of 0.80 and decreases to 9 × 10^{-11} m² at a porosity of 0.65. The permeability-porosity relationship tends to shift to the upper left of Figure 6, which means in the snow being easier to densify and that permeability increases as the snow ages. For example, at a given porosity of 0.6, the permeability would be equal to 5 × 10^{-11} m² on January 27th while it would be equal to 4 × 10^{-9} m² on April 2nd, which corresponds to increase of 2 orders of magnitude.

3.3 Thermal conductivity measurements

The results of the thermal conductivity measurements are plotted versus porosity in Figure 7. Thermal conductivity of the different samples ranged from 0.09 to 0.48 W/mK for snow porosities between 0.42 and 0.80. As expected, measured thermal conductivity of snow decrease with increasing porosity since air thermal conductivity (0.03 W/(m·K) at -10°C) is lower than that of ice (2.33 W/(m·K)). The results of this study compare very well with data from the literature as shown by the pale gray dots (Sturm et al. 1997, Lachance 2014).

The trend lines drawn in Figure 7 are used to indicate the slope variation with age. Indeed, an increase in the slope can be observed over time. This will be further discussed in section 4.

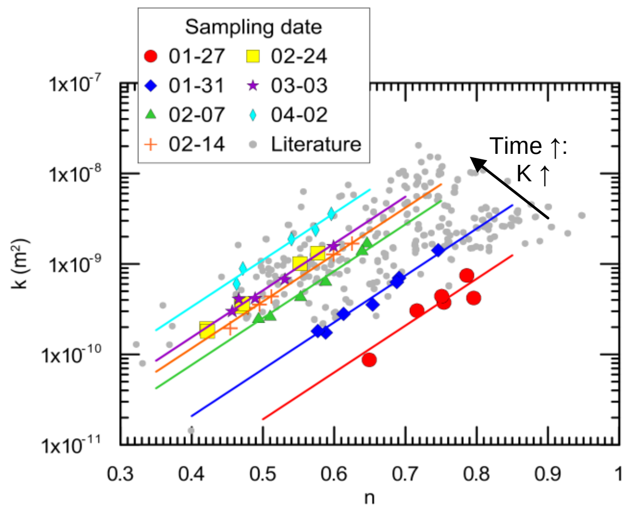

Figure 6. Intrinsic permeability versus porosity for all the snow samples.

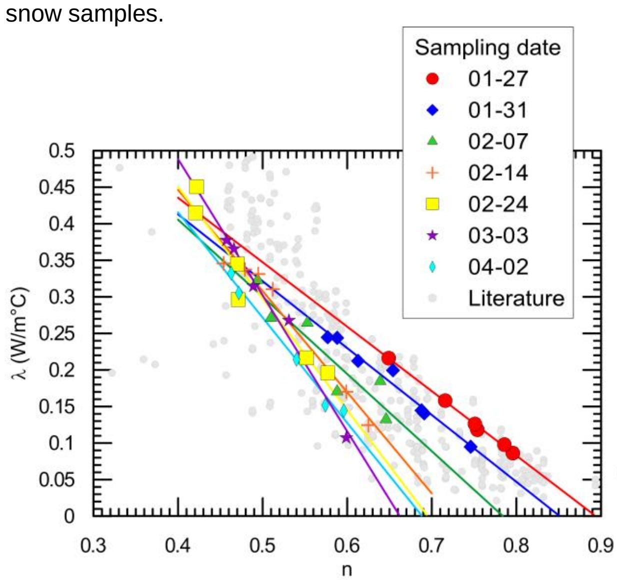

Figure 7. Thermal conductivity versus porosity of all the snow samples.

4 DISCUSSION

4.1 Equivalent sphere radius

As shown on Figure 6, a model based on porosity only cannot estimate the intrinsic permeability for all snow type. Shimizu (1970) has established the first model with the density and diameter of grain as parameters:

$$k = 0.077 d^2 \cdot \exp\left(-7.8\rho^*\right) \qquad [3]$$

where d is the mean grain size (cm) and ρ* is the normalized snow density (with reference to water density). Calonne (2012) used the same exponential mathematical form to obtain different regression coefficients from 3-D image-based computed permeability results:

$$k = 3.0 \cdot r_{es}^2 \cdot \exp\left(-0.013 \cdot \rho\right) \qquad [4]$$

where r_{es} is the equivalent snow flake radius (m) Since the physical diameter has not been measured in this study, it was left as a variable parameter and was computed using the least squares regression method. The colored regression lines plotted in Figure 6 were all obtained from equation 4 and the fairly narrow fit to the experimental data from each sampled batches demonstrates that eq. [4] is particularly suited to represent snow permeability. Diameters estimated in this manner are consistent with those obtained experimentally from the literature (Shimizu 1970, Hardy and albert 1993). Table 2 presents the ranges for the individually calculated r_{es} and the r_{es} computed using least square method with corresponding SSA (m²/kg) calculated using the following equation:

$$SSA = \frac{3}{r_{es} \cdot \rho_i} \qquad [5]$$

where ρ_i is the ice density (917 kg/m^3). The individual equivalent diameters ranged from 0.08 mm to 0.81 mm with corresponding calculated SSA from 81 m^2/kg to 9 m^2/kg.

Table 2. Calculated equivalent sphere radius and SSA from individual measurement and from least square methode corresponding to the sampling date and age of the snow.

Sampling date	Age range at testing (days)	r_{es} range (mm)	r_{es} least square (mm)	SSA least square (m^2/kg)
27 Jan	2-5	0.04-0.06	0.05	67
31 Jan	8-12	0.09-0.10	0.09	35
07 Feb	12-19	0.17-0.20	0.18	18
14 Feb	22-26	0.21-0.23	0.22	15
24 Feb	29-37	0.24-0.27	0.26	13
03 Mar	38-47	0.25-0.28	0.26	13
02 Apr	66-75	0.35-0.40	0.38	9

4.2 Temporal evolution of equivalent grain size and specific surface area

The calculated equivalent sphere radiuses from individual snow samples and average SSAs corresponding to each sampled batch are plotted versus time in Figure 8 and 9, respectively. As expected, the equivalent sphere radius increases over time while the specific surface area decreases. The growth rate of the snow grains is higher on fresher snow batches. In fact, grain sizes of snow samples from January 27th and January 31st tends to increase although kept at isothermal condition after sampling (insulated box in a -18 °C cold room). This behavior is caused by the erosion of the snow grains which may starts as a highly dendritic snowflake and progressively morphs into an ice sphere and may be affected by compaction conditions. Each following samples do not seem to be affected by compaction conditions and by aging effect in stored conditions as the radiuses tend to stay constant during the 4 to 5 days of testing, as respectively shown by the light green, red, pink, yellow, orange and dark green dots.

Morin et al. (2013) described the metamorphism process with three different parameters, dendricity, sphericity and grain size as implemented in the crocus model. Results from this model (Crocus) are also presented on figure 9 for a thermal gradient of 10 °C/m, the average thermal gradient of this study being fairly close (-11.6 °C/m). Legagneux et al. (2003) proposed the following logarithmic fit and parameters:

$$SSA(t) = B - A \cdot \ln(t + \Delta t) \qquad [6]$$

where A and B are empirical parameters (m^2/kg), t is the elapsed time (hour) and Δt is a time correction parameter (hour). Using the measured data from this study with the least square method on equation 6, the obtained parameters are 8.95 m²/kg for A, 71.86 m²/kg for B and -0.92 days for Δt with a determination coefficient R^2 of 0.981. These values agree well with those of Taillandier (2006) for snow under similar thermal gradients.

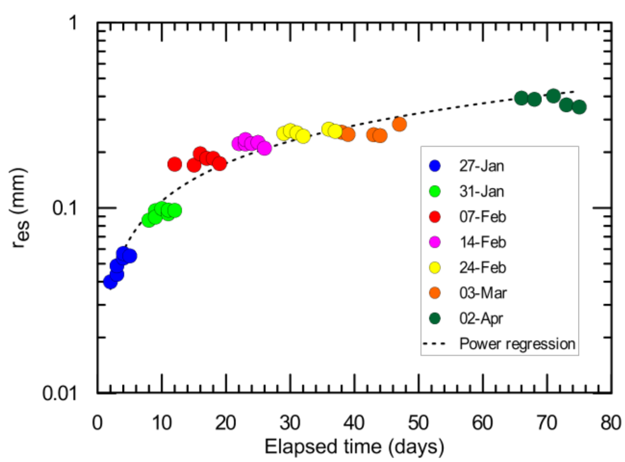

Figure 8. The equivalent sphere radius for individual measurements versus elapsed time in days.

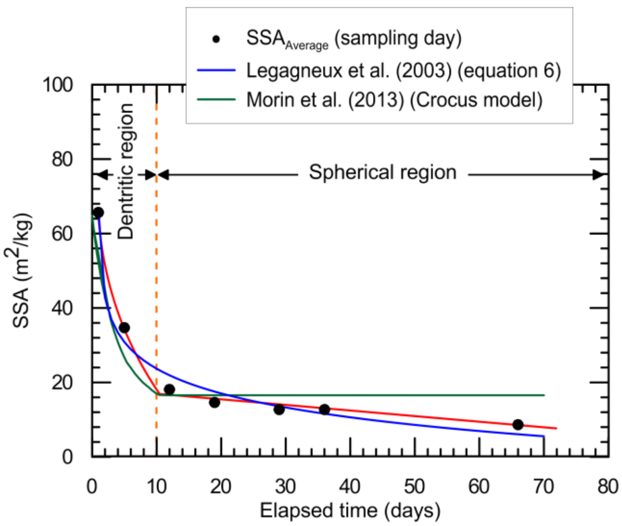

Figure 9. The specific surface area versus elapsed time in days with a best fit for each region (red line), Legagneux et al. (2003) model (blue line) and Crocus results for a thermal gradient of 10°C/m from Morin et al. (2013).

4.3 Effect of the manual compaction to thermal conductivity results.

While thermal conductivity of snow does not generally depend on snow grain diameter (Sturm et al. 1997, Côté et al. 2012), a slight structural effect can be observed by the trend lines on Figure 7 since the slope of the thermal conductivity versus porosity is steeper for older snow than for the freshly precipitated snowflake. This effect may be caused by the formation of small thermal ices bridges between flakes. Friction during compaction would allow partial snow melting at contact points immediately refreezing to form an ice cement bond increasing thermal efficiency. This effect tends to decrease with time as particle naturally becomes more spherical making it more difficult to create those ice bonds.

This ice bond effect does not seem to affect permeability measurements which could be tentatively explained by the relatively small bond volume compared to the pore volume.

5 CONCLUSION

A laboratory study of the evolution of the thermal conductivity and intrinsic permeability of compacted snow was conducted on samples collected at Laval University at the same location but at different times throughout the winter of 2014. Two apparatuses, a needle probe and an air permeameter, were used to measure thermal conductivity and intrinsic permeability on 41 different samples of various densities out of 7 sampled batches of the same snow layer. As expected, the experimental results indicated that the intrinsic permeability of compacted snow increased while thermal conductivity decreased for an increasing porosity. These results compared well with the data available from the literature.

The empirical model from Calonne et al. (2012) was employed to determine an equivalent sphere radius based on measured permeability and porosity. The resulting diameters were of the same order of magnitude as measured values from available literature. The computed r_{es} and SSAs also allowed a quantification of the aging process. Legagneux et al. (2003) equation 6 was used to predict SSA since the parameters A, B and Δt compared with previous work. In summary, it has been possible to establish an SSA decay function with time of the studied snow cover using the relationship between intrinsic permeability and porosity together with the Calonne et al. (2012) model. Finally, a structure effect was observed on thermal conductivity which may be caused by thermal bonds among the remaining dendrites of snowflakes.

The results of this study will be integrated in an upcoming snow property model to help consider snow covers in thermal analysis of civil infrastructures in cold and moderately cold regions.

ACKNOWLEDGEMENTS

This study was supported by the NSERC Research Chair on Life-Cycle Assessment of Embankment Dams. The authors wish to acknowledge François Gilbert and Christian Juneau for their help in the development of the measurement apparatuses.

REFERENCES

Arakawa, H., Izumi, K., Kawashima, K., Kawamura, T. 2009. Study on quantitative classification of seasonal snow using specific surface area and intrinsic permeability, *Cold Region Science and Technology*, doi:10:1016 /j.coldregions.2009.07.004.

Bader, H. 1939. Mineralogical and structural characterization of snow and its metamorphism, *Snow and Its Metamorphism*, SIPRE Translation pp. 1-55.

Carman, P.C. 1956. *Flow of gases through porous media*, Academic Press, New York, NY, USA.

Calonne, N., Geindreau, C., Flin, F., Morin, S., Lesaffre, B., Rolland du Roscoat, S., Charrier, P. 2012. 3-D image-based numerical computations of snow permeability: links to specific surface area, density, and microstructural anisotropy, *The Cryosphere*, 6, 939–951.

Colbeck, S.C., Akitaya, E., Armstrong, R.L., Gubler, H., Lafeuille, J., Lied, K., McClung, D.M., Morris, E.M. 1990. The International Classification for Seasonal Snow on the Ground. *International Commission on Snow and Ice (IAHS)*, World Data Center A for Glaciology, University of Colorado, Boulder, CO, USA.

Côté, J., Rahimi, M., Konrad J.-M. 2012. Thermal conductivity of compacted snow, *15th International Conference on Cold Regions Engineering*, Quebec, Canada.

Dominé, F., Lauzier, T., Cabanes, A., Legagneux, L., Kuhs, W.F., Techmer, K., Heinrichs, T. 2003. Snow metamorphism as revealed by scanning electron microscopy. *Microscopy Research and Technique.* 62, 33-48. doi: 10.1002/jemt.10384.

Hardy, J.P., Albert, D.G. 1993. The permeability of temperate snow, Preliminary links to microstructure, *50th eastern snow conference and 61st western snow conference*, Quebec City, Québec, Canada.

Jaffar, H., Picot, J.J. 1970. Thermal conductivity of snow by a transient State probe method, *Water Resources Research*, 6 (1), 333-335.

Lachance, O., Côté, J., Gosselin, L., Konrad, J.-M. 2013. Heat and mass transfer properties of compacted snow, *GeoMontreal 2013*, 66e conférence annuelle canadienne de géotechnique et 11e conférence conjointe SCG/AIH sur les eaux souterraines, Montréal, QC.

Lachance, O. 2014. Propriétés du transfert thermique et de masse de la neige compactée, *Mémoire*, Université Laval, Québec, 101p.

Legagneux, L., Lauzier, T., Dominé, F., Kuhs, W.F., Heinrichs, T., Techmer, K. 2003. Rate of decay of specific surface area of snow during isothermal experiments and morphological changes studied by scanning electron microscopy, *Canadian Journal of Physics*, 81, 459-468.

Morin, S., Domine, F., Arnaud, L., Picard, G. 2010. In-situ monitoring of the time evolution of the effective thermal conductivity of snow. *Cold Regions Science and Technology*, 64, 73-80.

Morin, S., Domine, F., Dufour, A., Lejeune, Y., Lesaffre, B., Willemet, J. M., Carmagnola, C.M., Jacobi, H. W. 2013. Measurements and modeling of the vertical profile of specific surface area of an alpine snowpack, *Advances in Water Resources*, 55, 111–120.

Shimizu, H. 1970. Air permeability of deposited snow, *Contributions from the institute of low temperature science*, A 22, 1-32.

Sommerfeld, R.A., Rocchio, J.E. 1993. Permeability measurements on new equitemperature snow. Water Resources Resources Research, 38(8), 2485-2490.

Sturm, M., Johnson, J.B. 1992. Thermal conductivity measurements of depth hoar, *Journal of Geophysical Research*, 97(B2), 2129-2139.

Sturm, M., Holmgren, J., König, M., Morris, K. 1997. The thermal conductivity of seasonal snow, *Journal of Glaciology*, 43, 26–41.

Sturm, M., Benson, C.S. 1997. Vapor transport, grain growth and depth-hoar development in the subarctic snow. , *Journal of Glaciology*, 43, 42-59.

Taillandier, A.-S. 2006. Evolution de la surface spécifique de la neige. Etudes expérimentales et de terrain, paramétrisation. *Thesis*, Université Joseph Fourier, Grenoble, 263p.